Preprints of the 2012 20th Mediterranean Conference on Control & Automation (MED), Barcelona, Spain, July 3-6, 2012

Robust Estimation and Control of Tire Traction Forces

Tesheng Hsiao, *Member, IEEE*

***Abstract*—This paper proposes a tire traction force control scheme which effectively deals with the highly nonlinear and uncertain tire-road interaction, and variations in road conditions. Moreover, the proposed control scheme is based on robust estimations of traction forces; therefore, unlike the slip-ratio-based methods, achievement of desired traction forces is guaranteed by the proposed control scheme. Then simulations are conducted for verification. The results show that the performance of traction force estimation and control is satisfactory, even under the conditions of suddenly changed tire-road friction-coefficients and mismatched tire models for controller design and simulations.**

I. INTRODUCTION

Driving safety and performance can be significantly improved if tire traction forces are under careful control. Tire traction force control has been implemented in production vehicles in a variety of forms. For example, traction control systems (TCSs) and antilock braking systems (ABSs) are effective in preventing tires from spinning or skidding under adverse conditions such as acceleration or deceleration on wet or icy roads; direct yaw control (DYC) is realized by applying additional braking forces to stabilize the yaw motion of the vehicle [1, 2].

Control of tire traction forces is challenging in many aspects. Firstly, the tire-road interaction is complicated, highly nonlinear and uncertain. Many tire models, including dynamic/static and analytical/empirical models [3], have been proposed to elucidate the mechanism of tire force generation; however each of them considers only parts of the tire behavior (e.g. speed dependency or hysteresis). Moreover, it is difficult to know in advance or to estimate on-line the parameters associated with the tire models. Therefore, tire-model-based control schemes inevitably suffer from considerable uncertainties of both model parameters and model structures.

Sliding mode control and fuzzy logic control have been found useful in dealing with uncertain nonlinear systems. Lee and Tomizuka [4] investigated both approaches and concluded that the sliding mode controller performed better if a reliable tire model was available, while the fuzzy logic controller was preferable if the tire model was unknown. Colli, *et al*. [5] also applied both methods to control the adherence gradient of tires and concluded that the sliding mode controller achieved slightly better performance. In addition, variations of sliding mode control such as the second-order sliding mode control [6, 7] and the dynamic surface control [8] were explored for their good robustness and reduced chattering phenomenon. A fuzzy logic ABS controller with separate rules for different road conditions was studied in [9].

Besides, Borrelli *et al*. implemented robust traction force control by modeling the nonlinear tire-road interaction as a hybrid system and applying model predictive control (MPC) to each continuous subsystem [10]. Gain-scheduled control [11] and mixed slip-deceleration (MSD) control [12] were proposed to robustly handle the nonlinear tire models.

The second challenging issue of traction force control is that the operational conditions of tires are time-varying and may change substantially. In particular, the road condition significantly affects generation of traction forces. To solve this problem, some traction force control laws relied on the aforementioned robust control techniques while some explicitly incorporated on-line estimations of the tire-road friction-coefficient. For example, the recursive least square algorithm with forgetting factor was used in [4], and the sliding mode observer was implemented in [6, 13].

The third challenge comes from immeasurability of tire traction forces; thus traction force control is accomplished indirectly by means of *slip ratio* control. Consequently, the control objectives of slip-ratio-based methods focused on tracking the desired slip ratio [4, 7], attaining maximum traction forces for fastest acceleration and deceleration [4-6, 13], or maintaining the slip ratio in the stable region, irrespective of road conditions [8].

However, the ever demanding requirements for driving safety inspire the need for precise traction force control. Recent studies have shown that coordinating traction forces of all tires in an optimal way improves yaw stability of the vehicle in sever situations (e.g. sharp cornering or braking on icy roads) [14-16]. Unfortunately, perfect slip ratio control does not guarantee achievement of desired traction forces. This is because uncertainties of tire models prohibit correct transfer of the desired traction force to the target slip ratio.

In view of the limitation of slip-ratio-based methods in high performance vehicle control systems, this paper turns to investigate direct traction force control with sufficient robustness margin. As a first step, a traction force estimator was developed which is robust w.r.t. tire model uncertainties and variations in road conditions. Then a controller based on the estimated force was proposed such that the desired traction force is attained. The proposed traction force control scheme takes the wheel torque as control input and generates desired traction forces. Therefore it can be seamlessly integrated into the advanced vehicle control systems, where the desired traction forces are evaluated by the yaw

Tesheng Hsiao is with the Department of Electrical Engineering, National Chiao Tung University, Hsinchu, 30010, Taiwan (TEL: 886-3-5131249; FAX: 886-3-5715998; e-mail: tshsiao@cn.nctu.edu.tw)

978-1-4673-2529-5/12/$31.00 ©2012 IEEE

stabilizing controller and then distributed optimally to each driven wheel [14-16]. Note that modern automotive technologies such as electronic limited-slip differentials (ELSD), torque-vectoring systems [17], and in-wheel motors [18] allow various degrees of freedom to independently control the torque of each driven wheel. Hence the proposed traction force control scheme is applicable to both internal combustion engine vehicles and electric vehicles.

The robust performance of the proposed estimator and controller was verified by simulations. The results showed that the actual traction force follows the desired one, despite sudden changes in road conditions and mismatched tire models used for controller design and tire simulations.

The rest of this paper is organized as follows: Section II introduces the tire models used in this paper. Section III presents the robust traction force estimator while the control algorithm is proposed in Section IV. Simulation results are presented in Section V and Section VI concludes this paper.

I. Model

In this paper, we assume that a vehicle is traveling along a straight line without cornering. One of the wheels is shown in Figure 1, which satisfies the moment balance equation:

$$I_w\dot{\omega} = T - F_x R$$

where T is the wheel torque, which is the sum of the braking torque and the engine torque transferred through the drivetrain. I_w, R, ω, and F_x are the moment of inertia, radius, rotational velocity, and traction force of the wheel, respectively. The deformation of the tire is neglected.

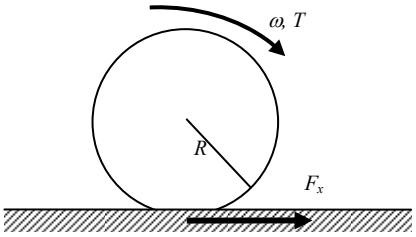

Figure 1: Tire rolling on a road surface

The traction force is closely related to the tire's slip ratio λ, which is defined as:

$$\lambda = \begin{cases} \dfrac{R\omega - v_w}{R\omega}, & \text{acceleration} \\ \dfrac{R\omega - v_w}{v_w}, & \text{braking} \end{cases}$$

where v_w is the translational velocity of the wheel. Since the vehicle is not turning, v_w is the same as the velocity of the vehicle's center of gravity (C.G.).

Many tire models have been proposed to describe the relation between the traction force and the slip ratio. One of the most popular tire models, called the magic formula [19], is a static empirical function of the slip ratio λ, tire-road friction- coefficient μ_p, and tire normal force F_z:

$$f_M(\lambda, \mu_p, F_z) = \mu_p D \sin\left\{C \tan^{-1}\left[B\lambda - E\left(B\lambda - \tan^{-1}(B\lambda)\right)\right]\right\} \quad (1)$$

where B, C, D, and E are parameters associated with the magic formula whose values vary with F_z. Note that F_z is not a constant when the vehicle is accelerating or decelerating due to the weight transfer effect.

Although the magic formula fits the experimental data reasonably well, it contains too many parameters which are usually unavailable in practice. Another simpler yet widely used tire model is the Dugoff model [20]:

$$f_D(\lambda, \mu_p, F_z) = C_x \frac{\lambda}{1-|\lambda|} k(s) \quad (2)$$

where $k(s) = \begin{cases} 1, & s \geq 1 \\ s(2-s), & s < 1 \end{cases}$ and $s = \dfrac{\mu_p F_z (1-|\lambda|)}{2C_x|\lambda|}$. C_x is the parameter associated with the Dugoff model. Since it is relatively easier to determine the parameter of the Dugoff model, we will use (2) with fixed C_x, μ_p and F_z as the nominal tire model for controller design, and use (1) to simulate the actual tire behavior. Note that we intentionally use different tire models for controller design and simulations in order to emphasize robustness of the proposed control scheme w.r.t. uncertainties in tire model structures.

The F_x-λ relation based on (1) for various μ_p and F_z are illustrated in Figure 2 (a) and (b), respectively. In addition, the F_x-λ relation based on (2) for μ_p =0.8 and F_z =4263 N are also shown in Figure 2 (a)(b) for comparison with (1).

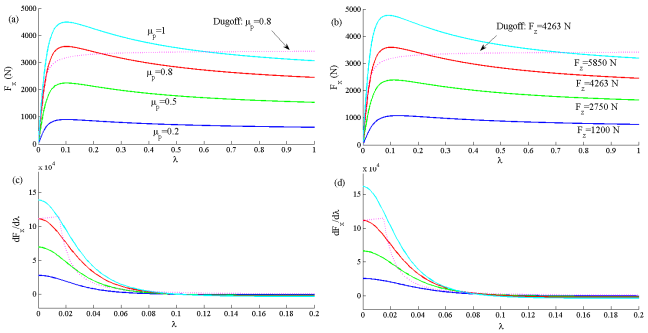

Figure 2: (a)(b): Graphs of F_x-λ based on the magic formula (solid line) and the Dugoff model (dotted line). F_z=4263 N for (a) and μ_p= 0.8 for (b). (c)(d): Graphs of $\frac{\partial F_x}{\partial \lambda}$ - λ based on the magic formula (solid line) and the Dugoff model (dotted line). F_z=4263 N for (c) and μ_p= 0.8 for (d).

II. Traction Force Estimation

A. Design of the Estimator

On designing the traction force estimator, we assume $F_x = f(\lambda, \mu_p, F_z)$, where f is an unknown function satisfying the following uncertainty bound:

$$\frac{\partial f(\lambda, \mu_p, F_z)}{\partial \lambda} = (1+\Delta)\frac{\partial f_0(\lambda)}{\partial \lambda}, \text{ and } |\Delta| \leq \bar{\Delta}, \ \forall \lambda, \mu_p, \text{and } F_z \quad (3)$$

where $f_0(\lambda) = f_D(\lambda, \mu_{p0}, F_{z0})$ is the Dugoff model evaluated at μ_p=μ_{p0} and F_z=F_{z0} for some fixed constants μ_{p0} and F_{z0}. f_0

will be treated as the nominal tire model for estimator and controller design. Δ is the model uncertainty bounded by a known constant $\bar{\Delta}$. Figure 2 (c) and (d) illustrate the $\frac{\partial f_M}{\partial \lambda}$-$\lambda$ relation based on the magic formula for various μ_p's. The $\frac{\partial f_0}{\partial \lambda}$ -λ relation is also presented in Figure 2 (c)(d) for comparison.

Then we define the normalized traction force as

$$\mu = \frac{F_x}{F_{z0}} \tag{4}$$

where F_{z0} is a constant.

Remark 1: Processing the derivative of the traction force may suffer from numerical problems since $\frac{\partial F_x}{\partial \lambda}$ is very large for small λ (see Figure 2(c)(d)); therefore normalization of F_x is preferred. Note that (4) differs from the common definition of *coefficient of traction* [21] in that the denominator of (4) is a constant, instead of the time-varying normal force F_z. According to (4), $\dot{\mu}$ and $\dot{F}_x$ are identical up to a normalization factor.

It is reasonable to assume that μ_p is quasi-static, then

$$\dot{\mu} = \frac{1}{F_{z0}}\left[\frac{\partial f}{\partial \lambda}\dot{\lambda} + \frac{\partial f}{\partial F_z}\dot{F}_z\right] \triangleq (1+\Delta)B(\mu,\lambda,v_w,\omega,T) + \frac{\partial f}{\partial F_z}\frac{\dot{F}_z}{F_{z0}} \tag{5}$$

where

$$B(\mu,\lambda,v_w,\omega,T) = \begin{cases} \frac{\partial f_0}{\partial \lambda}\frac{1}{F_{z0}\omega}\left[\frac{1-\lambda}{I_w}(T-\mu F_{z0}R) - \frac{\dot{v}_w}{R}\right], & \text{acceleration} \\ \frac{\partial f_0}{\partial \lambda}\frac{1}{F_{z0}v_w}\left[\frac{R}{I_w}(T-\mu F_{z0}R) - (1+\lambda)\dot{v}_w\right], & \text{braking} \end{cases} \tag{6}$$

If $\omega, v_w, \dot{v}_w$ and T are available, then the proposed traction force estimator is

$$\dot{\hat{\mu}} = B(\hat{\mu},\lambda,v_w,\omega,T) + \eta(\phi) \tag{7}$$

$$\dot{\phi} = \Phi \tag{8}$$

$$\dot{\hat{\omega}} = \frac{T - \hat{\mu}F_{z0}R}{I_w}, \quad \hat{\omega}(0) = \omega(0) \tag{9}$$

ϕ is an auxiliary state of the estimator, and η is a function of ϕ which is to be determined. To simplify the notation, we denote $B = B(\mu,\lambda,v_w,\omega,T)$ and $\hat{B} = B(\hat{\mu},\lambda,v_w,\omega,T)$.

Define the error signals: $e_\mu = \mu - \hat{\mu}$ and $e_\omega = \omega - \hat{\omega}$. Note that $e_\mu = -\frac{I_w}{RF_{z0}}\dot{e}_\omega \triangleq \dot{e}_I$, i.e. $e_I = -\frac{I_w}{RF_{z0}}e_\omega$ is proportional to e_ω and is the integration of e_μ.

We make the following assumptions:

$$|e_\mu(t)| \le E_\mu(t) \text{ for all } t \ge 0 \tag{10}$$

$$\text{and} \quad \left|\frac{\partial f}{\partial F_z}\frac{\dot{F}_z}{F_{z0}}\right| \le \Gamma, \text{ for all } \lambda, \mu_p, \text{ and } F_z \tag{11}$$

Γ and $E_\mu(t)$ are given constant and function of time, respectively. Assumption (10) is feasible because $|F_x| \le F_z$ and thus there exists one trivial $E_u = \frac{F_z}{F_{z0}} + |\hat{\mu}|$. Section III.B will discuss the procedure for evaluating a tighter upper bound of $|e_\mu|$ based on e_I.

From (5) and (7) we have

$$\dot{e}_\mu = (1+\Delta)A_0 e_\mu + \Delta\hat{B} + \frac{\partial f}{\partial F_z}\frac{\dot{F}_z}{F_{z0}} - \eta \tag{12}$$

where

$$A_0 = \begin{cases} -\frac{\partial f_0}{\partial \lambda}\frac{R}{\omega}\frac{1-\lambda}{I_w}, & \text{acceleration} \\ -\frac{\partial f_0}{\partial \lambda}\frac{1}{v_w}\frac{R^2}{I_w}, & \text{braking} \end{cases}$$

Let $\tilde{\phi} = \phi - e_I$. Then consider the following Lyapunov function:

$$V_E(e_\mu, e_I, \tilde{\phi}) = \frac{1}{2}\gamma_1 e_\mu^2 + \frac{1}{2}\gamma_2 e_I^2 + \frac{1}{2}\gamma_3\tilde{\phi}^2$$

where γ_1, γ_2, γ_3 are positive constants. Clearly, $V_E \ge 0$ for all e_μ, e_I and $\tilde{\phi}$. $V_E = 0$ if and only $e_\mu = e_I = \tilde{\phi} = 0$. Then

$$\begin{aligned} \dot{V}_E &= \gamma_1 e_\mu \dot{e}_\mu + \gamma_2 e_I e_\mu + \gamma_3(\phi - e_I)(\Phi - e_\mu) \\ &= \gamma_1\left((1+\Delta)A_0 e_\mu^2 + \hat{B}\Delta e_\mu + \frac{\partial f}{\partial F_z}\frac{\dot{F}_z}{F_{z0}}e_\mu - \eta e_\mu\right) + \gamma_2 e_I e_\mu \\ &\quad + \gamma_3(\phi - e_I)(\Phi - e_\mu) \\ &\le (\gamma_1(1+\Delta)A_0 - \alpha_1)e_\mu^2 + \alpha_1 e_\mu^2 + (\gamma_2 e_I - \gamma_3(\phi - e_I) - \gamma_1\eta)e_\mu \\ &\quad + \gamma_1\left(|\hat{B}|\bar{\Delta} + \Gamma\right)E_\mu + \gamma_3(\phi - e_I)\Phi \end{aligned}$$

where $\alpha_1 > \frac{\beta_E\gamma_1}{2} + \gamma_1(1+\bar{\Delta})|A_0| > 0$ for some given positive constant β_E. Then $\gamma_1(1+\Delta)A_0 - \alpha_1 < 0$. Let

$$\begin{aligned} q(e_\mu) &= \alpha_1 e_\mu^2 + (\gamma_2 e_I - \gamma_3(\phi - e_I) - \gamma_1\eta)e_\mu + \gamma_1\left(|\hat{B}|\bar{\Delta} + \Gamma\right)E_\mu \\ &\quad + \gamma_3(\phi - e_I)\Phi + \frac{\beta_E}{2}\left[\gamma_2 e_I^2 + \gamma_3(\phi - e_I)^2\right] \\ &= \alpha_1 e_\mu^2 + be_\mu + c \end{aligned}$$

where $b = \gamma_2 e_I - \gamma_3(\phi - e_I) - \gamma_1\eta$ and $c = \gamma_1\left(|\hat{B}|\bar{\Delta} + \Gamma\right)E_\mu + \gamma_3(\phi - e_I)\Phi + \frac{\beta_E}{2}\left[\gamma_2 e_I^2 + \gamma_3(\phi - e_I)^2\right]$. If $q(e_\mu) \le 0$ for all $|e_\mu| \le E_\mu$, then $\dot{V}_E \le \beta_E V_E$. This implies that V_E converges to zero exponentially with the time constant $\frac{1}{\beta_E}$; i.e. $\hat{\mu} \to \mu$, $\hat{\omega} \to \omega$, and $\phi \to 0$ exponentially. Because $q(e_\mu)$ is a convex parabolic function of e_μ, one sufficient condition for $q(e_\mu) \le 0$ for all $|e_\mu| \le E_\mu$ is

$$b \le 0 \quad \text{and} \quad q(-E_\mu) \le 0 \tag{13}$$

The graphical interpretation of (13) is illustrated in Figure 3. Rearranging (13) yields

$$\begin{aligned} \gamma_2 e_I - \gamma_3(\phi - e_I) \le \gamma_1\eta \le \frac{1}{E_\mu}\{&-\alpha_1 E_\mu^2 + (\gamma_2 e_I - \gamma_3(\phi - e_I))E_\mu \\ &-\left[\gamma_1\left(|\hat{B}|\bar{\Delta} + \Gamma\right)E_\mu + \gamma_3(\phi - e_I)\Phi + \frac{\beta_E}{2}\left[\gamma_2 e_I^2 + \gamma_3(\phi - e_I)^2\right]\right]\} \end{aligned} \tag{14}$$

If we choose

$$\Phi = -\left[\frac{\alpha_2}{\gamma_3}E_\mu + \frac{\beta_E}{2}\right](\phi - e_I) - \frac{\alpha_1 E_\mu^2 + \gamma_1\left(|\hat{B}|\bar{\Delta} + \Gamma\right)E_\mu + \frac{\beta_E}{2}\gamma_2 e_I^2}{\gamma_3(\phi - e_I)} \tag{15}$$

where $\alpha_2 > 0$ and

$$\eta = \tfrac{1}{\gamma_1}\left[\gamma_2 e_I - \gamma_3(\phi - e_I) + \tfrac{1}{2}\alpha_2(\phi - e_I)^2\right]$$

then (14), or equivalently (13), holds. This implies that $\dot{V}_E \le \beta_E V_E$ and then $e_\mu \to 0$ exponentially.

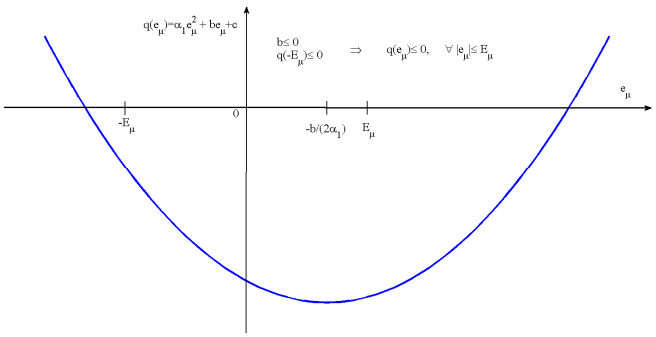

Figure 3: $q(e_\mu)$ and the graphical interpretation of (13).

Remark 2: As t approaches infinity, the denominator of the second term in (15) approaches zero. Therefore (15) is modified such that the absolute value of the denominator is no less than some predefined positive number ε. Consequently, (14) may be violated for small estimation errors. In such a case, only ultimate boundedness of the estimation error is achieved.

B. *Upper Bound of the Estimation Error*

Although there exists a trivial E_μ which satisfies assumption (10), we want E_μ as small as possible for a less stiff differential equation (15). To do this, we first evaluate the filtered estimation error. Let $G(s) = \frac{a}{s+a}$, a>0, and

$$\tilde{p}(s) = G(s)\tilde{e}_\mu(s) = sG(s)\tilde{e}_I(s)$$

where the notation $\tilde{\bullet}(s)$ denotes the Laplace transform of the time domain function $\bullet(t)$. Because $sG(s)$ is proper, p can be obtained by filtering e_I. Let $G_d(z) = \frac{1-a_d}{1-a_d z^{-1}}$ be the discrete-time approximation of $G(s)$ [22] with impulse response $g_d[k] = (1-a_d)a_d^k$ for $k \in \mathbb{Z}^+$, where $a_d = e^{-aT_s}$, and T_s is the sampling time. Let $p(0)$=0, $p[k] = p(kT_s)$, and $e_\mu[k] = e_\mu(kT_s)$; then

$$|p[k]| = |(g_d * e_\mu)[k]| \le \|e_\mu\|_{k\infty}\|g_d\|_1 \qquad (16)$$

where $*$ denotes the discrete-time convolution, $\|\bullet\|_1$ is the l_1-norm, and $\|e_\mu\|_{k\infty} \triangleq \max_{0\le m\le k}|e_\mu[m]|$.

On the other hand, let δ_d be the *discrete-time impulse signal*. Then the triangle inequality and (16) imply that

$$\|e_\mu\|_{k\infty} - \|p\|_{k\infty} \le \|e_\mu - p\|_{k\infty} = \|(\delta_d - g_d) * e_\mu\|_{k\infty} \le \|\delta_d - g_d\|_1 \|e_\mu\|_{k\infty}$$

where $\|\delta_d - g_d\|_1 = 2a_d$. If $a > \frac{\ln 2}{T_s}$, then $a_d < \frac{1}{2}$. We have

$$|e_\mu[k]| \le \|e_\mu\|_{k\infty} \le \frac{1}{d}\|p\|_{k\infty} \qquad (17)$$

where $d = 1 - \|\delta_d - g_d\|_1 = 1 - 2a_d > 0$. (17) is an upper bound of $|e_\mu(t)|$ at t=kT_s. If T_s is sufficiently small, we can assume that $|e_\mu(t)| \le \frac{1}{d}\|p\|_{k\infty}$ for $kT_s \le t < (k+1)T_s$.

Note that $\|p\|_{k\infty}$ is a non-decreasing function of time; however the estimation error decays exponentially. Consequently, (17) will be over-conservative as t increases. Hence, we replace $\|p\|_{k\infty}$ by the *recent maximum value* of $|p|$ and allow this maximum value to decay exponentially with the time constant $\frac{1}{\beta}$, where $\beta < \beta_E$. The flowchart in Figure 4 illustrates the procedure for calculating $E_\mu(t)$.

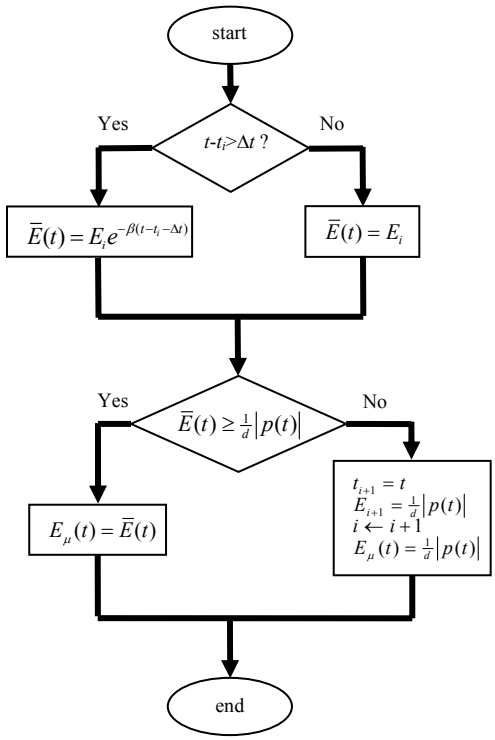

Figure 4: flowchart of evaluating the $E_\mu(t)$

In Figure 4, Δt defines the time window within which the historical maximum value of $|p|$ is searched and preserved. E_i, i=0,1,2,…, denotes the latest historical maximum value of $|p|$ taking place at time t_i. The initial values for t_0 and E_0 are set to be zeros.

III. Traction Force Control

Given the desired traction force F_{xd}, we want to determine the wheel torque T such that $F_x \to F_{xd}$. Consider the following wheel torque:

$$T = \begin{cases} F_{xd}R + \dfrac{I_w}{1-\lambda}\left[\dfrac{\dot{v}_w}{R} + \dfrac{\omega}{\frac{\partial f_0}{\partial \lambda}}\left(\dot{F}_{xd} - \varsigma\right)\right], & \text{acceleration} \\ F_{xd}R + \dfrac{I_w}{R}\left[(1+\lambda)\dot{v}_w + \dfrac{v}{\frac{\partial f_0}{\partial \lambda}}\left(\dot{F}_{xd} - \varsigma\right)\right], & \text{braking} \end{cases} \qquad (18)$$

where ζ is to be determined. Define the tracking error $e_t = F_x - F_{xd}$ and substitute (18) into (6). Then we get

$$B = \frac{1}{F_{z0}}\left(A_0 e_t + \dot{F}_{xd} - \varsigma\right) \text{ and } \hat{B} = \frac{1}{F_{z0}}\left(A_0(\hat{F}_x - F_{xd}) + \dot{F}_{xd} - \varsigma\right) \quad (19)$$

Moreover,

$$\dot{e}_t = (1+\Delta) A_0 e_t + \Delta \dot{F}_{xd} + \frac{\partial f}{\partial F_z}\frac{\dot{F}_z}{F_{z0}} - (1+\Delta)\varsigma \quad (20)$$

Let $e_a = \hat{F}_x - F_{xd} = e_t - e_\mu F_{z0}$. Then from (12), (19), and (20) we have

$$\dot{e}_a = A_0 e_a - \varsigma + \eta F_{z0}$$

Now consider the following Lyapunov function:

$$V\left(e_a, e_\mu, e_I, \tilde{\phi}\right) = \tfrac{1}{2} e_a^2 + V_E\left(e_\mu, e_I, \tilde{\phi}\right)$$

It is obvious that $V \geq 0$ for all e_a, e_μ, e_I, and $\tilde{\phi}$. $V=0$ if and only if $e_a=0$ and $V_E=0$, which in turn implies that $e_t=e_\mu=e_I=\tilde{\phi}=0$. The time derivative of V is

$$\dot{V} = e_a\left(A_0 e_a - \varsigma + \eta F_{z0}\right) + \dot{V}_E$$

If we choose

$$\varsigma = \kappa e_a + \eta F_{z0}$$

where $\kappa \geq \frac{\beta_t}{2} + A_0$, for some $0 < \beta_t < \beta_E$. Then

$$\dot{V} = (A_0 - \kappa) e_a^2 + \dot{V}_E \leq -\tfrac{\beta_t}{2} e_a^2 - \beta_E V_E \leq -\beta_t\left(\tfrac{1}{2} e_a^2 + V_E\right) = -\beta_t V$$

Therefore $\hat{F}_x$ converges to F_{xd} exponentially with the time constant $\frac{1}{\beta_t}$. Since $F_x - \hat{F}_x = e_\mu F_{z0}$ is at least ultimately bounded, we conclude that the tracking error e_t is also ultimately bounded.

Remark 3: We assume that the F_{xd} comes from an upper layer controller which determines that total traction force required for maintaining a stable trajectory of the vehicle, and distributes the total traction force to each driven wheel in a feasible way according to the road conditions. Therefore F_{xd} is achievable.

IV. Simulations

A. Setting

We consider that the proposed traction force control scheme is implemented in the rear wheels of a rear-wheel-drive vehicle. Assume that two of the rear wheels are identical. Then the vehicle's longitudinal dynamics is modeled as

$$ma_x = 2F_x$$

where m is the mass of the vehicle, a_x is the acceleration of the vehicle's C.G. and F_x is the traction force of a single rear wheel.

Choose $F_{z0} = \frac{1}{4}mg$ and the normal force of the rear wheel is

$$F_z = \frac{m}{2}\frac{g l_f + a_x h}{l_f + l_r}$$

where l_f and l_r are the distances from the vehicle's C.G. to the front and rear axle respectively. h is the height of the vehicle's C.G. g is the gravitational acceleration. The values of these parameters are set to be m=1740kg, l_f=1.05m, l_r=1.4m, and h=0.7m. Note that the proposed traction force control scheme needs not to know these parameters.

The radius and the moment of inertia of the wheel are set to be R=0.3m and I_w=2.03N·m^2. The magic formula whose parameters are taken from [23] is used to simulate the tire behavior. The nominal tire model is $f_0(\lambda)=f_D(\lambda,\mu_{p0}, F_{z0})$, where μ_{p0}=0.8 and f_D is the Dugoff model with C_x=111169 N.

In practice, the uncertainty bounds $\bar{\Delta}$ and Γ should be determined from experimental data. In this simulation, they are obtained by numerically searching the values of the magic formula and the Dugoff model over a presumed range. By definition, $\lambda \in [-1,1]$, and we assume that $\mu_p \in [0.2, 1]$, which represents the road conditions from icy roads to dry asphalt roads. Besides, we assume $F_z \in [1200\text{N}, 7400\text{N}]$, which allows more than 1g longitudinal acceleration. The search result suggests that $\bar{\Delta}$=32 and Γ=0.1858.

Other design parameters are listed in Table 1. Besides, Zero-mean Gaussian noises are added to the measurements of v_w, $\dot{v}_w = a_x$, and ω such that their signal-to-noise ratios (SNRs) are around 20 dB.

Table 1: Design Parameters.

Estimator		Evaluation of E_μ		Controller
α_2=0.5	γ_1=500	a=200	T_s=0.005sec	β_t=20
β_E=50	γ_2=5000	β=10	Δt=0.2sec	
	γ_3=10			

B. Results

The simulation results are illustrated in Figure 5 and Figure 6. The tire-road friction-coefficient μ_p is shown in Figure 5(a). We assume that μ_p=0.9 for the first 10-second period, μ_p=0.2 for the next 10-second period, and μ_p=0.5 for the last 10-second period. The desired traction force is

$$F_{xd}(t) = 600\sin(2t) \text{ N}, \quad t \geq 0$$

F_{xd}, F_x, and $\hat{F}_x$ are shown in Figure 5(c). It can be seen that the performance of estimation and control is satisfactory. Figure 5(d) presents the (unnormalized) estimation error $F_x - \hat{F}_x = e_\mu F_{z0}$ and the tracking error $e_t = F_x - F_{xd}$. Since $e_t \approx e_\mu F_{z0}$, the desired result $e_a \to 0$ is attained. The transient responses of e_t and e_μ resulting from sudden changes of road conditions vanish quickly (less than 0.1 sec) and then the system is stabilized again. Although the tracking error increases on the low-friction road surface, its peak-to-peak amplitude is still less than 5% of the peak-to-peak amplitude of the desired traction force.

Since the control objective is to follow the sinusoidal F_{xd}, the wheel torque generated by the controller (see Figure 5(b)) is also sinusoidal with constant amplitude, while the amplitude of the slip ratio (see Figure 6(a)) changes corresponding to the tire-road friction-coefficients.

Figure 6(b) shows the wheel rotational velocity ω and its estimates $\hat{\omega}$ from (9). The measured rotational velocity is also shown in Figure 6(b). Convergence of the error $e_\omega = \omega - \hat{\omega}$ is achieved. The absolute estimation error $|e_\mu|$ and its upper bound E_μ are shown in Figure 6(c). It shows that the upper bound proposed in Section III.B is valid and reasonable. Figure 6(d) is the normal force F_z, which varies with the

traction force. These simulation results illustrate that the proposed traction force estimator and controller possess robust performance w.r.t. model uncertainties, changes of road conditions, and variations in normal forces.

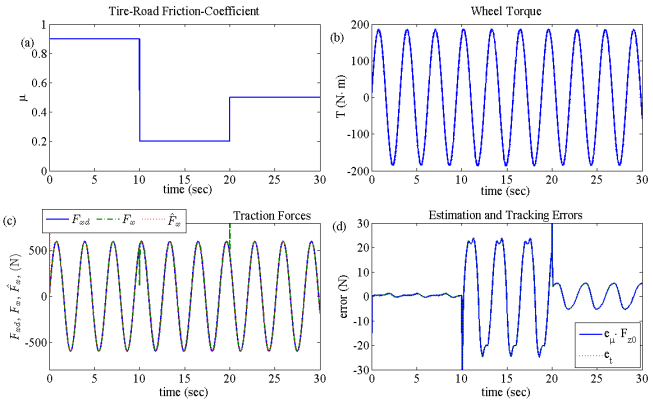

Figure 5: (a): tire-road friction-coefficient μ_p (b): wheel torque T (c): F_{xd} (solid line), F_x (dash-dot line), and $\hat{F}_x$ (dotted line) (d): (unnormalized) estimation error $e_\mu F_{z0}$ (solid line) and tracking error e_t (dotted line).

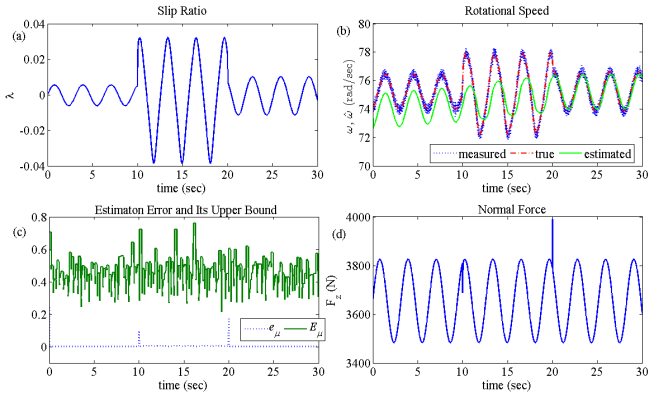

Figure 6: (a): slip ratio λ (b): ω (true: dotted line, measured: dash-dot line), $\hat{\omega}$ (solid line) (c): absolute estimation error $|e_\mu|$ (dotted line) and its upper bound E_μ (solid line) (d): normal force F_z

V. Conclusion

Traction force control is usually accomplished by means of slip ratio control because the traction force is immeasurable. However, perfect slip ratio control does not guarantee achievement of the desired traction force due to tire model uncertainties. To solve this problem, this paper proposed a direct control scheme which is based on robust estimates of traction forces such that the desired traction force is attained, even under the conditions of uncertainties in tire model structures, and changes of the tire-road friction-coefficient. Satisfactory performance of the proposed estimator and controller was verified by simulations. Integrating the proposed control scheme into a higher layer yaw stabilizing control system will be the future research topic.

References

[1] C. Geng, *et al.*, "Direct Yaw-Moment Control of an In-Wheel-Motored Electric Vehicle Based on Body Slip Angle Fuzzy Observer," *IEEE Transactions on Industrial Electronics,* vol. 56, pp. 1411-1419, 2009.

[2] M. Canale, *et al.*, "Vehicle Yaw Control via Second-Order Sliding-Mode Technique," *IEEE Transactions on Industrial Electronics,* vol. 55, pp. 3908-3916, 2008.

[3] L. Li, *et al.*, "Integrated Longitudinal and Lateral Tire/Road Friction Modeling and Monitoring for Vehicle Motion Control," *IEEE Transactions on Intelligent Transportation Systems,* vol. 7, pp. 1-19, 2006.

[4] H. Lee and M. Tomizuka, "Adaptive Vehicle Traction Force Control for Intelligent Vehicle Highway Systems (IVHSs)," *IEEE Transactions on Industrial Electronics,* vol. 50, pp. 37-47, 2003.

[5] V. D. Colli, *et al.*, "Single Wheel Longitudinal Traction Control for Electric Vehicles," *IEEE Transactions on Power Electronics,* vol. 21, pp. 799-808, 2006.

[6] M. Amodeo, *et al.*, "Wheel Slip Control via Second-Order Sliding-Mode Generation," *IEEE Transactions on Intelligent Transportation Systems,* vol. 11, pp. 122-131, 2010.

[7] M. Tanelli, *et al.*, "Traction Control for Ride-by-Wire Sport Motorcycles: A Second-Order Sliding Mode Approach," *IEEE Transactions on Industrial Electronics,* vol. 56, pp. 3347-3356, 2009.

[8] M. Kabganian and R. Kazemi, "A New Strategy for Traction Control in Turning Via Engine Modeling," *IEEE Transactions on Vehicular Technology,* vol. 50, pp. 1540-1548, 2001.

[9] G. F. Mauer, "A Fuzzy Logic Controller for an ABS Braking System," *IEEE Transactions on Fuzzy Systems,* vol. 3, pp. 381-388, 1995.

[10] F. Borrelli, *et al.*, "An MPC/Hybrid System Approach to Traction Control," *IEEE Transactions on Control Systems Technology,* vol. 14, pp. 541-551, 2006.

[11] T. A. Johansen, *et al.*, "Gain-Scheduled Wheel Slip Control in Automotive Brake Systems," *IEEE Transactions on Control Systems Technology,* vol. 11, pp. 799-811, 2003.

[12] S. M. Savaresi, *et al.*, "Mixed Slip-Deceleration Control in Automotive Braking Systems," *Journal of Dynamic Systems, Measurement, and Control,* vol. 129, pp. 20-31, 2007.

[13] G. A. Magallan, *et al.*, "Maximization of the Traction Forces in a 2WD Electric Vehicle," *IEEE Transactions on Vehicular Technology,* vol. 60, pp. 369-380, 2011.

[14] O. Mokhiamar and M. Abe, "Simultaneous Optimal Distribution of Lateral and Longitudinal Tire Forces for the Model Following Control," *Journal of Dynamic Systems, Measurement, and Control,* vol. 126, pp. 753-763, 2004.

[15] O. Mokhiamar and M. Abe, "How the Four Wheels should Share Forces in an Optimum Cooperative Chassis Control," *Control Engineering Practice,* vol. 14, pp. 295-304, 2006.

[16] J. Tjønnås and T. A. Johansen, "Stabilization of Automotive Vehicles Using Active Steering and Adaptive Brake Control Allocation," *IEEE Transactions on Control Systems Technology,* vol. 18, pp. 545-558, 2010.

[17] D. N. Piyabongkarn, *et al.*, "Active Driveline Torque-Management Systems," *IEEE Control Systems Magazine,* vol. 30, pp. 86-102, 2010.

[18] Y. Hori, "Future Vehicle Driven by Electricity and Control -- Research on Four-Wheel-Motored "UOT Electric March II"," *IEEE Transactions on Industrial Electronics,* vol. 51, pp. 954-962, 2004.

[19] H. B. Pacejka and E. Bakker, "The Magic Formula Tyre Model," *Vehicle System Dynamics,* vol. 21, pp. 1-18, 1993.

[20] R. Rajamani, *Vehicle Dynamics and Control*. New York: Springer, 2006.

[21] R. Rajamani, *et al.*, "Tire-Road Friction-Coefficient Estimation," *IEEE Control Systems Magazine,* vol. 30, pp. 54-69, 2010.

[22] G. F. Franklin, *et al.*, *Digital Control of Dynamic Systems*, 2 ed. New York: Addison-Wesley, 1990.

[23] J. Y. Wong, *Theory of Ground Vehicles*, 3 ed. New York: John Hiley & Sons. Inc., 2001.